第 50 卷 第 21 期/2023 年 11 月/中国激光 研究论文

中国激光

基于激光诱导自体荧光光谱的乳腺肿瘤特异性甄别

严剑锋[1]，李嘉源[1]，张幸[2]，谭俊[1]，傅进宇[1]，欧彩凤[3]，张成云[1]，罗云峰[2]，陈志峰[1*]，张普生[2**]

[1]广州大学物理与材料科学学院，广东 广州 510006；

[2]南方医科大学珠江医院乳腺外科，广东 广州 510280；

[3]广东药科大学附属第一医院乳腺科，广东 广州 510080

摘要 乳腺癌手术中常因缺乏快速准确的组织性质检测手段而导致组织过度切除或手术时间延长。利用组织自体光谱的检测手段因具有速度快、灵敏度高、选择性强以及无创性等优势而受到越来越多的关注。因此，针对乳腺癌寻求高效精准的光谱诊断特征并研究其内在根源具有重要意义。笔者以 355 nm 亚纳秒序列脉冲激光作为激发光源，采用自主搭建的激光诱导稳态荧光光谱系统对多例乳腺恶性肿瘤组织和正常乳腺组织开展自体荧光光谱实验研究。对两类组织样本的光谱特征进行比较分析，提出了基于 430 nm 附近光谱特征差异的特异性甄别方法，并比较了三种荧光比值法的甄别效果。进一步的光谱拟合分析揭示了实验测得的乳腺组织自体荧光主要来自 4 种内源性荧光物质的贡献，而癌变组织的光谱特征变化主要源于还原型辅酶Ⅰ（NADH）的增加以及 NADH 结合性蛋白的减少。本文提出的乳腺癌变光谱甄别方法特异性显著，生物学根源清晰，能够为临床快速检测应用提供新的技术方法参考，尤其是能为保乳手术中的切缘快速检测提供崭新的视角。

关键词 医用光学；自体荧光；乳腺肿瘤；稳态光谱；特异性甄别

中图分类号 TN247 **文献标志码** A **DOI**：10.3788/CJL230982

1 引 言

乳腺癌是严重威胁女性健康的第一大恶性肿瘤，国际癌症研究机构（IARC）2020 年的数据显示，其已超越肺癌成为全球发病率最高的癌症[1]。由于保乳手术在局部控制与长期生存率方面均与全乳切除相似，目前已经成为治疗早期乳腺癌的主要手术方法之一[2-4]。保乳手术成功的关键在于确保手术切缘无肿瘤病灶残留，并尽可能保留正常组织。目前，术中快速冰冻病理检查是乳腺癌术中检测手术切缘有无肿瘤残留的常用手段[5]。冰冻病理检查虽然可为临床医生提供可靠的诊断信息，但检测耗时较长（0.5～1 h），延长了手术时间与患者的麻醉时间，不利于患者的快速康复及医生的手术效率。此外，其准确性依赖于病理医师的知识经验水平，而且因仅检测手术切缘的代表性切片，存在敏感度较低、主观性强、非标准化等缺点。因此，探索能够实时、准确判断切缘组织良恶性的术中检测方法具有重大临床意义。

近年来，利用自体光谱技术检测组织病变的手段凭借速度快、灵敏度高、选择性强以及无创性等优势[6]，逐渐被人们关注，在肿瘤相关检测中具有广阔的应用前景[7-8]。Shapey 等[9]通过分析 5 种人类脑肿瘤和 9 种不同类型的正常脑组织在 400～1800 nm 波段的吸收光谱，研究了其体外光学特性，得出肿瘤的散射系数明显不同于周围正常组织的结论。糜岚研究团队[10]运用无标记自体荧光光谱技术检测了宫颈癌和癌前病变，敏感性和特异性分别达到了 100% 和 91%。Benoit 等[11]发现利用 405 nm 激光诱导的自体荧光特征峰分析可以准确区分良性和潜在恶性进化的肝结节，灵敏度达到 84%。目前已有少量工作对乳腺组织病变的自体光谱检测开展了探索，如：Gupta 等[12]利用波长为 337 nm 的 N_2 气体激光器激发乳腺组织的自体荧光，发现基于荧光绝对强度便可对恶性乳腺肿瘤、良性乳腺肿瘤和正常乳腺组织进行区分；丁建华等[13]采用波长为 488 nm 的激光激发诱导乳腺肿瘤与正常乳腺组织的自体荧光光谱，也找到了光谱中存在的甄别特征；高天欣等[14]探讨了乳腺疾病在近红外图像中的表现规律，并提出了根据血红蛋白对近红外光的特异性吸收判断肿瘤增生部位和良恶性的检测方法。然而，当前针对乳腺肿瘤的自体光谱检测、甄别仍不够准确，对于

收稿日期：2023-07-03；**修回日期**：2023-07-28；**录用日期**：2023-08-10；**网络首发日期**：2023-08-15

基金项目：国家自然科学基金（11974085）、广东省自然科学基金（2020A1515010411）、广东省高等教育教学改革项目（2019-N466）、广州市科技计划项目（2023A03J0125）、北京“新锐肿瘤支持治疗课题研究”公益项目（cphcf-2022-076）、广东省大学生创新训练项目（S202011078105，S202111078099）

通信作者：*chenzf@gzhu.edu.cn；**zhangpusheng@smu.edu.cn

一些已发现的光谱特征差异也尚未明确其内在机制[15-16]。因此，进一步寻求高效精准的光谱诊断特征并揭示其内在根源，对于临床快速诊断仍具有重要意义。

本课题组根据人体组织常见内源性荧光基团的激发波长范围[17-19]以及组织自体荧光强度弱的特点，选取 355 nm 的亚纳秒序列脉冲激光作为激发光源，采用自主搭建的激光诱导稳态荧光光谱系统对乳腺恶性肿瘤组织和正常乳腺组织的自体荧光光谱开展了实验研究。基于对两类组织样本的光谱特征对比，提出了新的特异性甄别方法，并展示了三种荧光比值法的甄别效果。此外，通过光谱拟合分析进一步揭示了癌变组织光谱特征变化的生物学根源。

2 实验测试

2.1 实验样本

实验测试样本是由南方医科大学珠江医院课题组提供的非特殊浸润性乳腺癌患者切除的乳房腺体。术中医生从切除下来的乳房腺体中切取体积约为 10 mm^3 的癌变组织以及正常腺体组织（切除边缘）薄片，样本采集过程中注意避开血污、脂肪等。待检组织不经任何处理，用石英玻片夹持固定，在 3～5 ℃条件下保存，并在样本离体 8 h 内完成光谱检测实验。本实验共检测样本 10 例，乳腺癌变组织和正常腺体组织各 5 例，每例检测 2 个位点，最后取有效测试的 18 组数据（癌变组织和正常组织各 9 个位点）进行对比分析。

2.2 实验装置

为了研究乳腺癌变组织和正常乳腺组织在特定激光源激发下的自体荧光光谱的特异性，采用一套自主搭建的激光诱导稳态荧光光谱系统进行光谱检测实验。如图 1 所示，波长为 355 nm、脉宽为 500 ps、重复频率为 1 kHz 的固体脉冲激光器（RealLight MCC-355-1-25）发出的激光脉冲序列，经过可调衰减器衰减后，以平均功率 1 mW（脉冲能量 1 μJ）通过透镜聚焦激发实验样本，样本表面的激发光斑直径约为 500 μm。由于组织的自体荧光非常弱，选择亚纳秒脉冲激光作为激发源，有利于在较低的平均光功率下获得良好的信噪比，且不会对样本造成不可逆损伤。所激发的样本自体荧光由两个透镜组成的透镜组进行收集，以获得更优的收集率以及耦合孔径角。荧光经过截止波长为 380 nm 的介质型长波通滤光片滤除其中的激发光成分后，耦合进入光栅光谱仪（Zolix Omni-λ200i）进行光谱分光，该系统的光谱分辨力可达 0.1 nm，光谱测量范围为 200～900 nm。最后，光谱信号经由光电倍增管（Zolix PMTH-S1V1-CR131）进行光电转换，由单光子计数型数据采集器进行采集。为避免激发光通过透镜及玻片后产生非预期的荧光背景信号，实验中均使用石英玻璃制作的透镜及玻片。所有光谱检测实验均在温度为 23 ℃、相对湿度为 40% 的环境下进行。

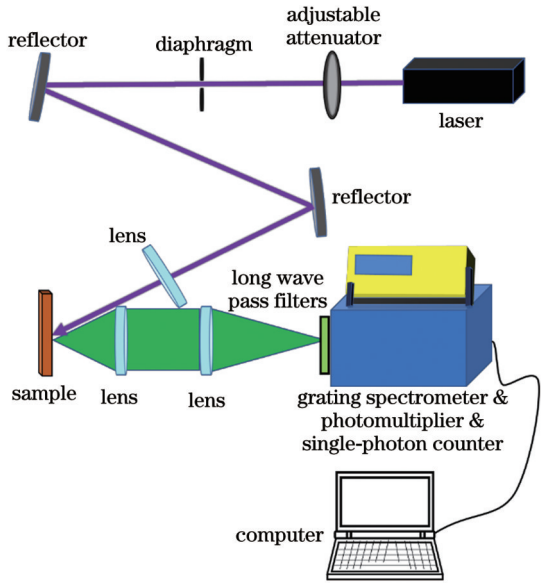

图 1 激光诱导稳态荧光光谱实验系统

Fig. 1 Experimental system for laser-induced steady fluorescence spectroscopy

3 实验结果与分析讨论

3.1 光谱特征对比

研究表明，当正常组织转变成恶性肿瘤组织后，其内部生化环境会发生质的变化。因此，当正常腺体组织发生癌变后，组织中各种荧光基团的含量和分布会发生变化，导致稳态荧光光谱特征发生改变，具体表现为荧光特征峰的位移与强度发生变化。图 2 所示为正常乳腺腺体组织与乳腺恶性肿瘤组织的激光诱导稳态自体荧光光谱，为方便对比观察，对图中部分曲线的纵坐标进行了不同程度的缩放。

由图 2（a）可见，正常乳腺组织的自体荧光光谱曲线基本呈现双峰结构，除了短波方向存在一个较平缓的荧光峰外，在 465 nm 或 495 nm 附近存在较为明显的荧光峰，个别曲线在 455 nm 处出现了微小的凹陷。图 2（b）所示的乳腺恶性肿瘤组织的自体荧光光谱曲线呈现出更明显的双峰结构，其峰值分别在 400 nm 和 465 nm 附近，400 nm 处的荧光峰较之正常乳腺而言更为突出。值得注意的是，这些曲线在 430 nm 处都可以看到程度不一的凹陷，而正常乳腺组织的所有光谱曲线在 430 nm 附近均没有出现凹陷。可以认为这是两类样本之间最直观的光谱特征差异。

3.2 特异性甄别

根据上述光谱特征，本课题组尝试利用两类组织光谱在 430 nm 附近的凹陷特征差异进行特异性甄别。因为乳腺恶性肿瘤的光谱曲线在 400 nm 和 465 nm 附近均呈现荧光峰，而正常乳腺腺体的光谱曲线在该两处也均具有较大的相对强度，故运用荧光比值法是一个理想的选择。对比了 I_{430}/I_{465}、I_{430}/I_{400} 以及 $2I_{430}/(I_{400}+I_{465})$ 比值法的结果，如图 3（a）～（c）所示。容易看出：相比于乳腺恶性肿瘤，正常乳腺腺体的 I_{430}/I_{465} 和 I_{430}/I_{400}

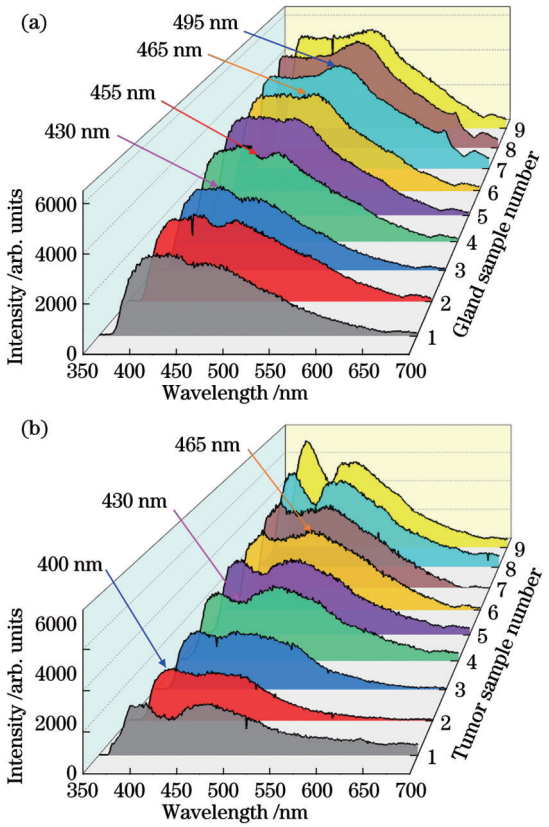

图 2 正常乳腺腺体组织与乳腺恶性肿瘤组织的激光诱导稳态自体荧光谱。(a)正常乳腺腺体组织;(b)乳腺恶性肿瘤组织

Fig. 2 Laser-induced steady autofluorescence spectra of normal breast gland tissues and breast malignant tumor tissues. (a) Normal breast gland tissues; (b) breast malignant tumor tissues

值更高,但这两个比值尚不能很好地区分两类组织;$2I_{430}/(I_{400}+I_{465})$比值具有更好的区分效果,若以 0.95 作为甄别阈值,则可以对所有样本测试点实现 100% 甄别。因此,针对乳腺癌变,本课题组认为 $2I_{430}/(I_{400}+I_{465})$荧光比值法是具有可行性的光谱特异性甄别方法。

3.3 光谱成分分析

如上所述,自体荧光光谱变化的根源是细胞组织病变所致的组织形态变化、代谢水平变化以及微环境变化等,最终导致光激发空间范围内的各种内源性荧光基团的含量发生改变。

在光谱分析中经常会用到高斯模型,采用高斯函数拟合荧光光谱可以得到组织中荧光基团的光谱特征信息[20]。本课题组运用式(1)所示的多项高斯函数对实验测得的自体荧光光谱进行拟合分析。

$$I=\sum_{i=1}^{n}\frac{A_i}{w_i\sqrt{\pi/2}}\exp\left[-2\left(\frac{\lambda-\lambda_i}{w_i}\right)^2\right], \tag{1}$$

式中:下标 i 表示叠加的高斯型光谱的编号;A_i 为积分面积;w_i 为标准全宽;λ_i 为中心波长。图 4 所示光谱是同类采样光谱数据的归一化平均值,遵循最低

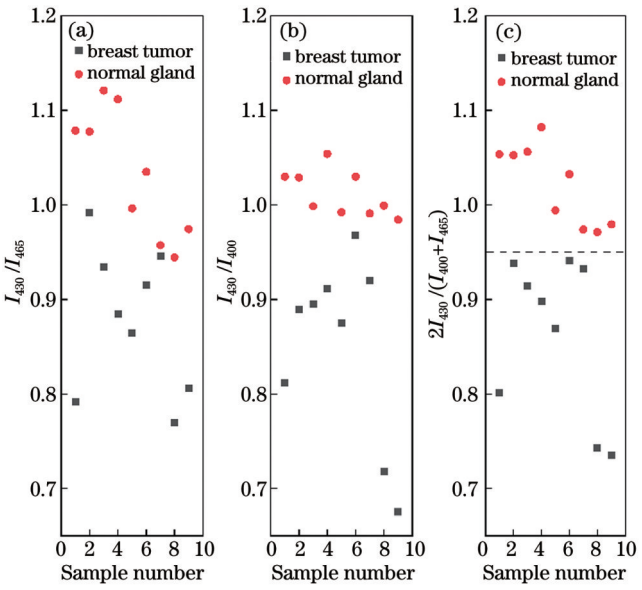

图 3 三种荧光比值法对正常乳腺腺体和乳腺恶性肿瘤的甄别效果。(a)I_{430}/I_{465}荧光比值法;(b)I_{430}/I_{400}荧光比值法;(c)$2I_{430}/(I_{400}+I_{465})$荧光比值法

Fig. 3 Identification effect of three fluorescence ratio methods on normal breast glands and breast malignant tumors. (a) I_{430}/I_{465} fluorescence ratio method; (b) I_{430}/I_{400} fluorescence ratio method; (c) $2I_{430}/(I_{400}+I_{465})$ fluorescence ratio method

项数拟合原则,两类组织的自体荧光光谱曲线均可通过 4 项高斯叠加获得非常吻合的拟合结果(拟合校

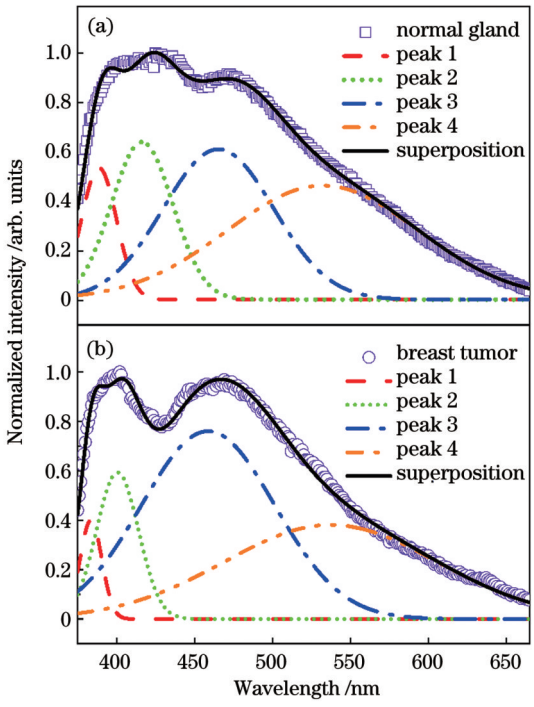

图 4 正常乳腺腺体光谱和乳腺恶性肿瘤光谱的高斯拟合分解。(a)正常乳腺腺体光谱;(b)乳腺恶性肿瘤光谱

Fig. 4 Gaussian decomposed fittings of normal breast glands and breast malignant tumors spectra. (a) Normal breast glands spectra; (b) breast malignant tumors spectra

正系数均在0.99以上)。光谱成分峰的积分比例以及中心波长的拟合值、标准误差见表1。对照人体常见内源性荧光基团的发射波长可知,所得的4个光谱成分峰中的前两个源于胶原蛋白和弹性蛋白的共同贡献,后两个则分别对应于还原型辅酶Ⅰ(NADH)以及黄素腺嘌呤[17-19]。因此,本实验中测得的乳腺组织自体荧光主要来自上述4种内源性荧光物质的贡献。

表1 光谱拟合结果及其对应的荧光基团

Table 1 Spectral fitting results and corresponding fluorophores

Tissue	Fitting results			
	Peak 1	Peak 2	Peak 3	Peak 4
Gland	8.8%±1.2% 389 nm±0.46 nm	18.4%±3.3% 416 nm±1.34 nm	31.4%±8.4% 465 nm±3.01 nm	41.3%±7.9% 532 nm±13.43 nm
Tumor	4.0%±0.6% 384 nm±0.31 nm	11.5%±0.9% 401 nm±1.23 nm	46.8%±6.8% 459 nm±1.20 nm	37.6%±8.0% 537 nm±18.92 nm
Fluorophore	Collagen+elastin		NADH	Flavin adenine

Notes: the data in the previous and next rows of the table are integral proportion±standard error and fitted wavelength±standard error, respectively.

结合图4和表1不难看出,上文分析得到的两类组织自体荧光光谱的主要特征差异,即乳腺恶性肿瘤在430 nm附近出现的光谱凹陷,主要源于Peak 3的变化:乳腺恶性肿瘤中的NADH含量较之正常乳腺组织有较显著的增加。Bonuccelli等[21]曾指出,NADH水平是癌症干细胞代谢水平的关键指标,其显著提高表示癌症干细胞活跃。Yu等[22]的研究显示,肿瘤中的NADH浓度是正常腺体的1.7倍,这与本文光谱拟合分析得到的结果非常接近。

此外,Rueck等[23]的工作表明,NADH与细胞内蛋白质结合会生成结合性蛋白,其发射荧光峰波长约为440 nm。Yu等[22]对比了正常乳腺细胞和乳腺肿瘤细胞的NADH水平,发现肿瘤细胞内线粒体电子传递链(ETC)酶受损使游离NADH明显多于正常细胞内的游离NADH,而结合性NADH占比减小。注意到在图4(a)和图4(b)中拟合所得的Peak 2的波长有较大差异,腺体的Peak 2在420 nm附近,而肿瘤的Peak 2在400 nm附近。此现象与上述报道的结论相符,Peak 2也有来自NADH结合性蛋白的贡献,正常腺体中的NADH结合性蛋白含量更高,使Peak 2峰值位置红移,同时强度增加。此外,肿瘤细胞中NADH结合性蛋白的减少对于430 nm附近的光谱凹陷也有一定的贡献。

4 结 论

选取355 nm亚纳秒序列脉冲激光作为激发源,采用自主搭建的激光诱导稳态荧光光谱系统对乳腺恶性肿瘤组织和正常乳腺组织开展了自体荧光光谱实验研究。通过对比两类组织样本的光谱特征,提出了基于430 nm附近凹陷特征差异的特异性甄别方法,通过$2I_{430}/(I_{400}+I_{465})$荧光比值法可以对乳腺癌变实现准确甄别。这意味着,实际应用中只要测量此三个特征波长下的荧光强度即可,这对于临床快速诊断十分有利。进一步的光谱拟合分析表明,实验测得的乳腺组织自体荧光主要来自4种内源性荧光物质的贡献,而癌变组织的光谱特征变化主要源于NADH的增加以及NADH结合性蛋白的减少。本工作提出的乳腺癌变光谱甄别方法特异性显著,生物学根源清晰,为临床快速检测应用提供了新的参考,尤其是为保乳手术中的切缘快速检测提供了崭新的视角。

参 考 文 献

[1] Sung H, Ferlay J, Siegel R L, et al. Global cancer statistics 2020: GLOBOCAN estimates of incidence and mortality worldwide for 36 cancers in 185 countries[J]. CA: a Cancer Journal for Clinicians, 2021, 71(3): 209-249.

[2] Gradishar W J, Moran M S, Abraham J, et al. Breast cancer, version 3.2022, NCCN Clinical Practice Guidelines in oncology[J]. Journal of the National Comprehensive Cancer Network, 2022, 20(6): 691-722.

[3] 宋尔卫, 陈凯, 刘荫华, 等. 中国早期乳腺癌保乳手术临床实践指南(2022版)[J]. 中国实用外科杂志, 2022, 42(2): 132-136.
Song E W, Chen K, Liu Y H, et al. Clinical practice guidelines of breast-conserving surgery for early breast cancer in China (2022 edition)[J]. Chinese Journal of Practical Surgery, 2022, 42(2): 132-136.

[4] Cardoso F, Kyriakides S, Ohno S, et al. Early breast cancer: ESMO Clinical Practice Guidelines for diagnosis, treatment and follow-up[J]. Annals of Oncology: Official Journal of the European Society for Medical Oncology, 2019, 30(8): 1194-1220.

[5] Mehdipour N Z, Navid O, Peyman A, et al. How accurate is frozen section pathology compared to permanent pathology in detecting involved margins and lymph nodes in breast cancer?[J]. World Journal of Surgical Oncology, 2021, 19(1): 261.

[6] 张洋, 何腾超, 刘林, 等. 基于离散三维荧光光谱的糖尿病识别方法研究[J]. 光学学报, 2022, 42(1): 0117002.
Zhang Y, He T C, Liu L, et al. Diabetes recognition method based on discrete three-dimensional fluorescence spectrum[J]. Acta Optica Sinica, 2022, 42(1): 0117002.

[7] 史晓凤, 马君, 毛伟征, 等. 最小二乘法分析自体荧光光谱识别胃癌[J]. 光谱学与光谱分析, 2006, 26(2): 295-298.
Shi X F, Ma J, Mao W Z, et al. Applying patial least-squares discriminant analysis on autofluorescence spectra to identify gastric

cancer[J]. Spectroscopy and Spectral Analysis, 2006, 26(2): 295-298.

[8] 吴拥军, 郝艳红, 吴维超, 等. 血清自体荧光光谱联合肿瘤标志物群在肺癌诊断中的价值[J]. 光谱学与光谱分析, 2009, 29(10): 2787-2791.
Wu Y J, Hao Y H, Wu W C, et al. Value of auto-fluorescence spectrum combined with tumor markers in diagnosis of lung cancer [J]. Spectroscopy and Spectral Analysis, 2009, 29(10): 2787-2791.

[9] Shapey J, Xie Y J, Nabavi E, et al. Optical properties of human brain and tumour tissue: an *ex vivo* study spanning the visible range to beyond the second near-infrared window[J]. Journal of Biophotonics, 2022, 15(4): e202100072.

[10] Jing Y Y, Wang Y L, Wang X Y, et al. Label-free imaging and spectroscopy for early detection of cervical cancer[J]. Journal of Biophotonics, 2018, 11(5): e201700245.

[11] Benoit C, Rodrigues A, Calderaro J, et al. Autofluorescence imaging within the liver: a promising tool for the detection and characterization of primary liver tumors[J]. European Radiology, 2022, 32(4): 2481-2491.

[12] Gupta P K, Majumder S K, Uppal A. Breast cancer diagnosis using N_2 laser excited autofluorescence spectroscopy[J]. Lasers in Surgery and Medicine, 1997, 21(5): 417-422.

[13] 丁建华, 余虹, 张志麟, 等. 离体乳腺正常组织、良性瘤及癌的自体荧光光谱[J]. 应用激光, 2000, 20(1): 38-39, 37.
Ding J H, Yu H, Zhang Z L, et al. Laser induced fluorescence spectra of normal, benign and malignant tissues of breast *in vitro* [J]. Applied Laser, 2000, 20(1): 38-39, 37.

[14] 高天欣, 范晓飞, 宣立学, 等. 乳腺癌的临床光谱检测[J]. 光谱学与光谱分析, 2008, 28(11): 2531-2535.
Gao T X, Fan X F, Xuan L X, et al. The clinical detection of breast cancer by spectrum method[J]. Spectroscopy and Spectral Analysis, 2008, 28(11): 2531-2535.

[15] Zhu C F, Palmer G M, Breslin T M, et al. Diagnosis of breast cancer using fluorescence and diffuse reflectance spectroscopy: a Monte-Carlo-model-based approach[J]. Journal of Biomedical Optics, 2008, 13(3): 034015.

[16] Volynskaya Z I, Haka A S, Bechtel K L, et al. Diagnosing breast cancer using diffuse reflectance spectroscopy and intrinsic fluorescence spectroscopy[J]. Journal of Biomedical Optics, 2008, 13(2): 024012.

[17] Li B H, Xie S S. Autofluorescence excitation-emission matrices for diagnosis of colonic cancer[J]. World Journal of Gastroenterology, 2005, 11(25): 3931-3934.

[18] 刘秉扬. 人体结肠组织的内源性荧光分子标记物研究[J]. 三明学院学报, 2011, 28(6): 60-64.
Liu B Y. Endogenous fluorophores of human colonic tissue *in vitro* [J]. Journal of Sanming University, 2011, 28(6): 60-64.

[19] Li B H, Zhang Z X, Xie S. Steady state and time-resolved autofluorescence studies of human colonic tissues[J]. Chinese Optics Letters, 2006, 4: 348-350.

[20] 陈文静, 教召航, 齐东丽, 等. 利用高斯函数拟合自体荧光光谱诊断乳腺癌的研究[J]. 中国激光, 2022, 49(20): 2007106.
Chen W J, Jiao Z H, Qi D L, et al. Study on diagnosis of breast cancer by fitting autofluorescence spectrum with Gaussian function [J]. Chinese Journal of Lasers, 2022, 49(20): 2007106.

[21] Bonuccelli G, de Francesco E M, de Boer R, et al. NADH autofluorescence, a new metabolic biomarker for cancer stem cells: identification of vitamin C and CAPE as natural products targeting "stemness"[J]. Oncotarget, 2017, 8(13): 20667-20678.

[22] Yu Q R, Heikal A A. Two-photon autofluorescence dynamics imaging reveals sensitivity of intracellular NADH concentration and conformation to cell physiology at the single-cell level[J]. Journal of Photochemistry and Photobiology B: Biology, 2009, 95(1): 46-57.

[23] Rueck A C, Hauser C, Mosch S, et al. Spectrally resolved fluorescence lifetime imaging to investigate cell metabolism in malignant and nonmalignant oral mucosa cells[J]. Journal of Biomedical Optics, 2014, 19(9): 096005.

Specific Identification of Breast Tumors Based on Laser-Induced Autofluorescence Spectroscopy

Yan Jianfeng[1], Li Jiayuan[1], Zhang Xing[2], Tan Jun[1], Fu Jinyu[1], Ou Caifeng[3], Zhang Chengyun[1], Luo Yunfeng[2], Chen Zhifeng[1*], Zhang Pusheng[2**]

[1]*School of Physics and Materials Science, Guangzhou University, Guangzhou* 510006, *Guangdong, China*;
[2]*Department of Breast Surgery, Zhujiang Hospital of Southern Medical University, Guangzhou* 510280, *Guangdong, China*;
[3]*Department of Breast Care Surgery, The First Affiliated Hospital of Guangdong Pharmaceutical University, Guangzhou* 510080, *Guangdong, China*

Abstract

Objective Breast cancer ranks highest in global incidence among all cancers, posing a significant threat to women's health. During surgical treatment for breast cancer, the absence of swift and precise tissue identification often results in either removal of excessive tissue or extended surgical durations. Recently, autologous tissue spectroscopy has garnered interest as a detection method due to its benefits, including speed, sensitivity, selectivity, and non-invasiveness. Consequently, identifying effective spectral diagnostic features for breast cancer and understanding their mechanisms are critically important.

Methods When normal tissue transforms into malignant tumor tissue, there is a qualitative shift in its internal biochemical environment. Hence, when normal glandular tissue undergoes carcinogenesis, the content and distribution of various fluorescent groups within that tissue alters, causing changes in the steady-state fluorescence spectral characteristics. In this study, a custom-built laser-induced steady fluorescence spectroscopy system was employed to conduct autofluorescence spectroscopy experiments on several malignant breast tumors and normal breast tissues (Fig. 1). A 355 nm sub-nanosecond sequence pulse laser served as the excitation light source. This choice was favorable for achieving a favorable signal-to-noise ratio at lower average optical power levels without inflicting irreversible damage to the samples. The constructed spectral system boasted a resolution as precise as 0.1 nm and spanned a spectral measurement range from 200 nm to 900 nm. The integration of a photomultiplier tube with a single-photon counter

facilitated the measurement of faint spectral signals.

Results and Discussions By comparing the spectral characteristics of the two types of tissue samples (Fig. 2), the spectral curves of tumors exhibit varying degrees of concave features near 430 nm, while all spectral curves of normal breast tissue samples show no concave features around 430 nm. This stands out as the most significant spectral characteristic difference between the two types of samples. We select 400, 430, and 465 nm as the spectral feature peaks and compare three ratio-based methods: I_{430}/I_{465}, I_{430}/I_{400}, and $2I_{430}/(I_{400}+I_{465})$. Based on this comparison, we propose that the fluorescence ratio method of $2I_{430}/(I_{400}+I_{465})$ serves as a feasible spectral-specific discrimination approach to differentiate between normal glandular tissue and breast tumors (Fig. 3). Using a discrimination threshold of 0.95, it is possible to realize 100% discrimination for all tested sample points.

Further spectral fitting analysis with Gaussian models shows that the experimental measurements of tumors and normal glandular tissue consist of four spectral components (Fig. 4). The autofluorescence of the breast tissue observed in the experiment predominantly stems from the contribution of four endogenous fluorescent substances: collagen, elastin, nicotinamide adenine dinucleotide hydrogen (NADH), and flavin adenine (Table 1). It is clear that the primary spectral characteristic difference in the autofluorescence spectra of the two types of tissues, as previously analyzed, namely, the spectral concavity observed near 430 nm in malignant breast tumors, primarily arises from the variation in peak 3. The heightened content of the reduced coenzyme NADH in malignant breast tumors when compared to normal breast tissue primarily explains this discrepancy. Moreover, a reduction in NADH-binding proteins leads to spectral variations in cancerous tissues.

Conclusions In this study, a 355 nm sub-nanosecond sequential pulsed laser is utilized as the excitation source and autofluorescence spectral experiments are performed on both malignant breast tumor tissue and normal breast tissue with a custom-built laser-induced steady-state fluorescence spectroscopy system. By comparing the spectral characteristics of these tissue types, we propose a specific discrimination method based on the distinct concave features observed near 430 nm. By computing the fluorescence ratio of $2I_{430}/(I_{400}+I_{465})$, breast cancer tissues can be precisely identified. Thus, to recognize breast cancer tissue, it is sufficient to measure the fluorescence intensity at these three key wavelengths and compute the corresponding fluorescence ratio. Further analysis using Gaussian models indicates that the breast tissue's autofluorescence predominantly stems from four endogenous fluorescent substances. The spectral shifts in cancerous tissues mainly arise from an increase in the reduced coenzyme NADH and a decrease in NADH-binding proteins. The breast cancer spectral discrimination approach introduced in this study demonstrates notable specificity and is underpinned by a clear biological rationale, presenting a new benchmark for swift clinical detection, especially valuable for margin evaluation during breast-conserving surgeries.

Key words medical optics; autofluorescence; breast tumor; steady spectroscopy; specific identification